

# lncRNA Chronos is an aging-induced inhibitor of muscle hypertrophy

Ronald L Nepl<sup>1,2</sup>, Chia-Ling Wu,<sup>1</sup> and Kenneth Walsh<sup>1</sup>

<sup>1</sup>Molecular Cardiology, Whitaker Cardiovascular Institute, Boston University School of Medicine, Boston, MA

<sup>2</sup>Department of Orthopedic Surgery, Brigham and Women's Hospital, Harvard Medical School, Boston, MA

Skeletal muscle exhibits remarkable plasticity in its ability to modulate its mass in response to the physiologic changes associated with functional use, systemic disease, and aging. Although a gradual loss of muscle mass normally occurs with advancing age, its increasingly rapid progression results in sarcopenia in a subset of individuals. The identities of muscle-enriched, long noncoding RNAs that regulate this process are unknown. Here, we identify a long noncoding RNA, named Chronos, whose expression in muscle is positively regulated with advancing age and negatively regulated during Akt1-mediated growth. Inhibition of Chronos induces myofiber hypertrophy both in vitro and in vivo, in part, through the epigenetic modulation of Bmp7 signaling.

## Introduction

Skeletal muscle accounts for 38–54% and 28–39% of total body mass in healthy men and women, respectively. These ranges are dependent on multiple factors, including age, physical activity level, nutritional input, overall health, and genetic makeup. Skeletal muscle comprises a heterogeneous mix of specialized myofibers that differ in their physiologic, metabolic, and biochemical attributes. On the ends of that spectrum are the slow, oxidative fibers of endurance athletes, comprising type I myosin heavy chain (MHC) proteins, and the fast, glycolytic fibers of power and strength athletes, comprising types IIa and IIx, and in rodents, IIb, MHC proteins. Interestingly, several clinical studies have demonstrated that resistance training, resulting in the maintenance of, and/or hypertrophy of, fast, glycolytic fibers can improve the cardiometabolic disease risk profile of patients with type 2 diabetes mellitus (LeBrasseur et al., 2011). Consistent with those findings, it is the fast, glycolytic fibers that atrophy at a greater rate than the slow, oxidative fibers during food deprivation, cancer-associated cachexia, glucocorticoid administration, and age-related sarcopenia (LeBrasseur et al., 2011; Ciciliot et al., 2013).

At the molecular level, the PI3K/Akt/mTOR signaling pathway has emerged as a key regulator of glycolytic muscle growth and metabolism in response to growth factors, insulin, resistance exercise, and nutritional input. Transgenic overexpression of Akt in skeletal muscle selectively promotes muscle hypertrophy (Lai et al., 2004), and its expression in glycolytic muscles promotes weight loss and insulin sensitivity in obese mice (Izumiya et al., 2008) and in aged mice that dis-

play a state of anabolic resistance and impaired activation of Akt (Akasaki et al., 2014). Functional overload (Bodine et al., 2001) and IGF-1 stimulation (Rommel et al., 2001; Takahashi et al., 2002) positively regulate PI3K/Akt/mTOR signaling in muscle and promote hypertrophy. Conversely, myostatin acts as a negative regulator of muscle hypertrophy, in part, through activation of an “atrogene” program (Cohen et al., 2015), and in part, by inhibiting PI3K/Akt/mTOR signaling (Sartori et al., 2009; Goodman and Hornberger, 2014). These molecular pathways converge on transcriptional programs that coordinate the cellular anabolic and catabolic processes mediated by changes in Smad signaling.

Advances in whole transcriptome sequencing have shown that >70% of the genome is actively transcribed (Lee, 2012) and that ~2 of every 3 transcripts do not encode for a protein (Iyer et al., 2015). Long noncoding RNAs (lncRNAs) are a class of genes, with little to no coding potential (Guttman et al., 2013), which are known to recruit chromatin-modifying complexes to genomic loci to regulate gene expression (Khalil et al., 2009; Guttman et al., 2011). Prior studies in cell culture have indicated that the lncRNAs MUNC (Mousavi et al., 2013; Mueller et al., 2015) and LncMyoD (Gong et al., 2015) promote myoblast differentiation and fusion in vitro by stimulating the transcription of MyoD, MyoG, and Myh3 and by negatively regulating the translation of Nras and Myc, respectively. However, the biological roles of lncRNAs in conditions of age-associated muscle atrophy have not, to our knowledge, been explored. Here, we describe a muscle-enriched lncRNA, called Chronos, which is negatively regulated by Akt signaling and positively regulated with advancing age. Chronos is shown

Correspondence to Ronald L. Nepl: rnepl@bwh.harvard.edu; Kenneth Walsh: kwwalsh@bu.edu

Abbreviations used: ChIP, chromatin immunoprecipitation; CTX, cardiotoxin; lncRNA, long noncoding RNA; MHC, myosin heavy chain; RIP, RNA immunoprecipitation; rTA, reverse tetracycline transactivator; siChronos, Chronos siRNA; siNC1, negative-control siRNA; STZ, streptozotocin; TA, tibialis anterior; TSS, transcriptional start site.

© 2017 Nepl et al. This article is distributed under the terms of an Attribution-Noncommercial-Share Alike-No Mirror Sites license for the first six months after the publication date (see <http://www.rupress.org/terms/>). After six months it is available under a Creative Commons License [Attribution-Noncommercial-Share Alike 4.0 International license, as described at <https://creativecommons.org/licenses/by-nc-sa/4.0/>].



to repress hypertrophic growth in vitro and in vivo, in part, by negatively regulating *Bmp7* expression.

## Results and discussion

Inducible overexpression of constitutively active Akt1 in type IIb glycolytic myofibers has been previously demonstrated to induce muscle hypertrophy and promote strength (Izumiya et al., 2008). RNAseq data obtained from that mouse model (Wu et al., 2017) was mined for lncRNAs, yielding numerous (~352) putative lncRNAs whose expression was significantly changed by the activation of the Akt1 transgene (Fig. 1 A). The lncRNA Gm17281, now referred to as Chronos, is significantly repressed in the hypertrophic muscle of TRE-myrAkt1/MCK-rtTA mice (Fig. 1, B and C). Northern blot analysis revealed marked enrichment of the ~3.6-kb Chronos transcript in skeletal muscle and heart, compared with other tissues (Fig. 1 D), and quantitative PCR analysis indicated Chronos is enriched in muscles with a greater percentages of type IIb glycolytic myofibers (Fig. 1 E), thus suggesting a biological role in striated muscle. To uncover the biological role of Chronos, its expression was examined in models of muscle regeneration and acute atrophy. Chronos expression is significantly decreased 14 d after cardiotoxin (CTX) injury of muscle (Fig. 1 F), a model that is associated with robust activation of Akt signaling (Zeng et al., 2010). Chronos expression is unchanged in the hind limb-unloading and type 1-diabetic mouse models, despite significant losses of gastrocnemius muscle mass (Fig. 1, G–J). Aging leads to a progressive loss of muscle mass in mice (Akasaki et al., 2014). Northern blot (Fig. 1 K) and quantitative PCR (Fig. 1 L) analysis revealed a progressive increase in Chronos expression with advancing age. Together, these data indicate that Chronos is an aging-related, Akt-inhibited lncRNA, whose expression is uncoupled from acute muscle loss.

To explore the biological role of Chronos, loss-of-function experiments were performed in myoblasts. Cells treated with Chronos siRNAs (siChronos), as compared with negative-control siRNAs (siNC1), display thicker and more highly branched MHC<sup>+</sup> myotubes by d 3, with clearly visible hypertrophy by d 3 and 5 (Fig. 2 A). To examine the biological role of Chronos in vivo, siNC1 was injected into either the left or right tibialis anterior (TA) muscle with the contralateral TA injected with either siChronos or siMyostatin. Immunofluorescence labeling of laminin and quantification of TA myofiber cross sections indicated siChronos treatment resulted in myofiber hypertrophy, as indicated by the flattening and rightward shift of the myofiber size-distribution curve (Fig. 2, B and C). In total, that treatment resulted in a significant, 42% increase in the mean myofiber cross-sectional area in the siChronos-treated mice (Fig. 2 D). Importantly, the biological effect of siChronos paralleled the effects of siMyostatin, which was used as a positive control (Kinouchi et al., 2008; Kawakami et al., 2013). Together, these data demonstrate that inhibition of Chronos expression results in hypertrophic growth both in vitro and in vivo.

To test the hypothesis that Chronos negatively regulates hypertrophic growth-factor signaling, the in vivo siRNA injections were repeated and assayed for changes in gene expression at the 7-d time point. Transcripts examined included members of the TGF- $\beta$  family; receptors for, and extracellular modulators of, those ligands; and other genes known to be involved in muscle growth processes (Miyazono et al., 2001). Of the 28 genes

examined, only *Bmp7*, *Fst*, *Acvr1b*, and *Gdf6* transcripts were significantly different among groups (Fig. 3 A and Fig. S1), with *Bmp7* displaying the most robust change in expression. During in vitro myogenesis, Chronos expression decreased on d 1–3, with its expression increasing to levels greater than that observed in proliferating myoblasts by d 5 (Fig. 3 B). Similar to in vivo observations, *Bmp7* transcript levels were robustly increased in differentiating myoblasts treated with siChronos as compared with siNC1 (Fig. 3 C). In addition, treatment with siChronos results in a nearly twofold increase in the induction of *Mef2a* (Fig. 3 D) and a subtle, but significant, increase in *MyoG* expression (Fig. 3 E) suggesting that Chronos has a role in regulating myogenesis in vitro.

*Bmp* signaling in general (Sartori et al., 2013), and the *Bmp7* ligand specifically (Winbanks et al., 2013), has been shown to positively regulate skeletal muscle hypertrophy through activation of Smad1/5. To corroborate the observed changes in *Bmp7* transcript levels, secreted *Bmp7* protein was quantified in differentiating myoblasts. Myoblasts treated with siChronos were found to secrete significantly more *Bmp7* protein as compared with controls (Fig. 3 F). Cell lysates from these cultures were assayed for the activating phosphorylation of the Smad1/5 and Smad2 signaling pathways. Consistent with a prior report (Clever et al., 2010), myoblast differentiation is associated with a steady decrease in pro-hypertrophic Smad1/5 phosphorylation (Fig. 3, G and H). Treatment with siChronos led to a robust and significant enhancement of Smad1/5 phosphorylation at days 3 and 4 of differentiation (Fig. 3, G and H). Further, inhibition of Chronos resulted in a consistent repression of anti-hypertrophic Smad2 phosphorylation at all time points (Fig. 3, G and I).

To further corroborate these observations, changes in protein synthesis and degradation were assayed on d 3–5 of differentiation. Differentiating myoblasts treated with siChronos displayed significant increases in puromycin incorporation, indicative of increased protein synthesis, as compared with siNC1 on d 3 and 4 of differentiation (Fig. 3, J–K). Next, ubiquitinated myosin was quantified in C2C12 cells on d 3–5 of differentiation as a measure of protein degradation. A decrease in ubiquitinated (coimmunoprecipitated) myosin was consistently observed in cells treated with siChronos as compared with siNC1 on d 4 and 5 (Fig. 3 L). Although a faint myosin signal was observed to be coimmunoprecipitated with ubiquitin on d 3 with siNC1 treatment, that was not quantified as the input signal was less than the detection threshold. Additionally, the effects of siChronos on protein synthesis in myotube cultures were examined. Myoblasts on d 4 of differentiation were treated with siChronos or siNC1 and assayed for puromycin incorporation. In that model, significant increases in protein synthesis were observed 48 and 72 h after treatment with siChronos (Fig. 3, M and N). Together, these results indicate that inhibition of Chronos biases the anabolic/catabolic signaling axis toward anabolic processes, perhaps through increased *Bmp7* signaling, in both developing and more-mature myotubes.

To extend those in vitro observations, the role of *Bmp7* in siChronos-mediated hypertrophy was tested in vivo. Transverse sections of TA muscles treated with siChronos, siChronos and siBmp7, and siNC1 were analyzed by immunofluorescence staining of laminin (Fig. 4 A). In agreement with earlier experiments (Fig. 2 C), siChronos treatment resulted in a flattening and a rightward shift of the myofiber size-distribution curve (Fig. 4 B) and an increase in the mean myofiber cross-sectional area (Fig. 4 C).

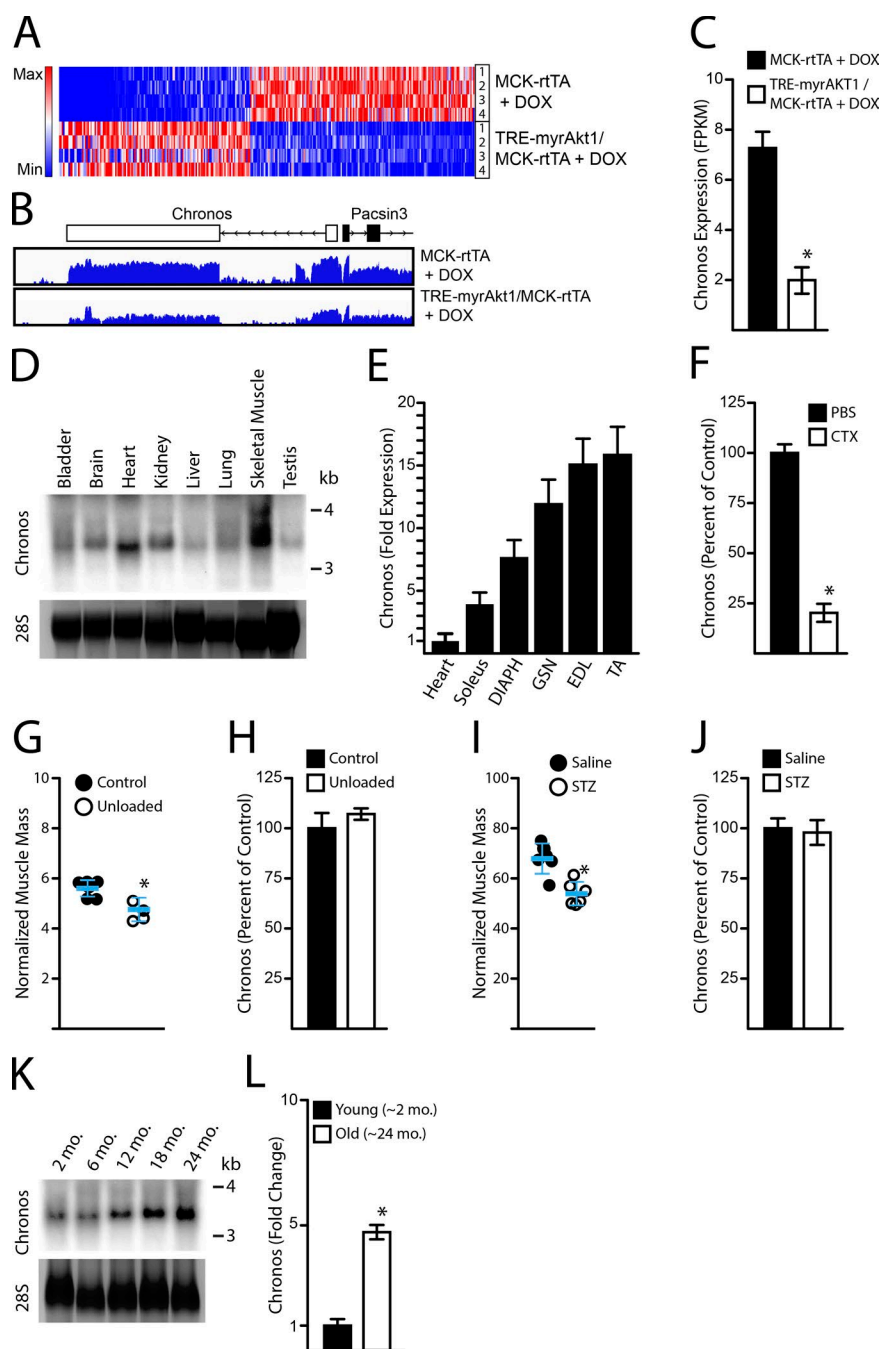


**Figure 1. Chronos is a growth-associated and muscle-enriched lncRNA.** (A) Heat map depicting differentially expressed lncRNAs from doxycycline-treated TRE-myrAkt1/MCK-rtTA and MCK-rtTA (control) mice. (B) RNAseq read profile of Chronos. Data are plotted on a  $\log_2$  scale. (C) Chronos expression (FPKM). \* $P < 0.05$  from  $n = 4$  TRE-myrAkt1/MCK-rtTA and  $n = 4$  MCK-rtTA mice. (D) Tissue distribution of Chronos in 2-mo-old mice. (E–J) Data are means  $\pm$  SD. (E) Chronos expression in the muscles of  $n = 3$  2-mo-old mice. (F) Chronos expression 14 d after CTX injury. \* $P < 0.05$  from  $n = 8$  independent experiments. (G and H) Hind limb unloading-induced muscle atrophy. \* $P < 0.05$  from  $n = 6$  control and  $n = 5$  unloaded mice. (I and J) Type 1 diabetes model of muscle atrophy. \* $P < 0.05$  from  $n = 6$  saline and  $n = 6$  STZ-injected mice. (K) Chronos expression in muscle from 2–24-mo-old mice. (L) Quantitative PCR analysis of Chronos expression in gastrocnemius muscle. \* $P < 0.05$  from  $n = 4$  young and  $n = 4$  aged mice. Data are means  $\pm$  SD.

tional area (Fig. 4 C). Co-injection of siBMP7 with siChronos resulted in significantly less hypertrophic growth as compared with siChronos treatment alone (Fig. 4 C). Collectively, these in vitro and in vivo observations are consistent with the notion that *Bmp7* functionally participates in the control of myofiber hypertrophy downstream of Chronos.

lncRNAs are known to recruit chromatin modifiers to genomic sequences, thereby regulating the epigenetic landscape and gene expression (Gupta et al., 2010; Hu et al., 2012; O'Leary et al., 2017; Pisignano et al., 2017). To assess the possibility that Chronos functions through a similar mechanism, we first performed an in silico alignment of Chronos with the *Bmp7* promoter (–10,000 nt) relative to the transcriptional start site (TSS). This analysis identified two sequences within Chronos, each with a high degree of sequence similarity to four

regions of the *Bmp7* promoter. A de novo motif search of the promoter region yielded an ~100-nt motif contained within each of the four homology regions identified in the in silico alignment. Together, those analyses identified two sequences of Chronos with antisense complementarity (77–85% similarity) to four genomic regions (denoted -7655, -7310, -6276, and -5494) that each contain the de novo identified motif (Fig. S2). To investigate the functional significance of those motifs, a 2.7-kb region encompassing the four genomic regions (-7950 to -5242), as well as two putative promoter sequences (-3674 to +3, and -1571 to +3) were subcloned into a promoter-less luciferase vector (Fig. 5 A). Luciferase activities were induced ~7–12-fold with the short and long *Bmp7* promoter sequences (Fig. 5 B), thus indicating promoter activity in the context of myoblast differentiation. Addition of siChronos had no effect

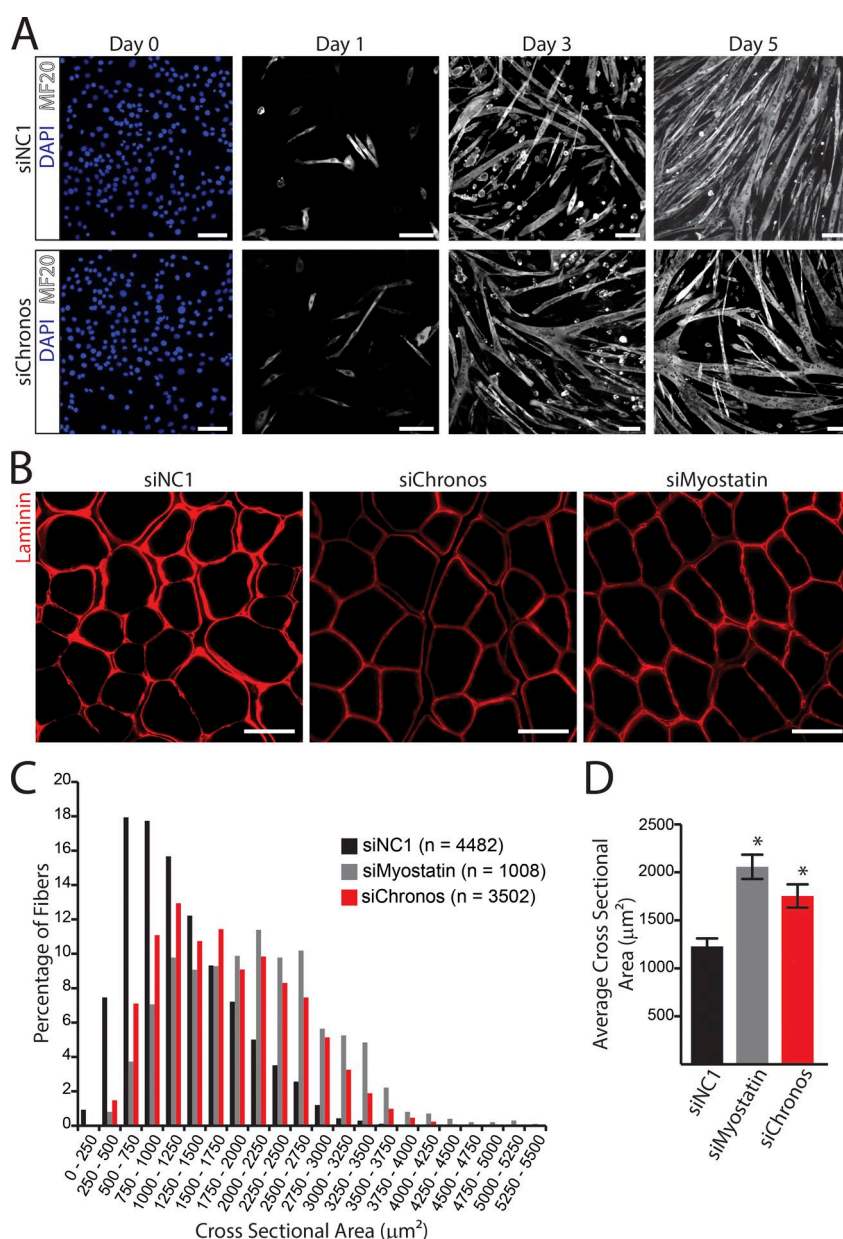


**Figure 2. Inhibition of Chronos results in hypertrophic growth.** (A) Immunostaining of myoblasts during in vitro differentiation. Bars, 100  $\mu$ m. (B–D) Inhibition of Chronos in vivo. Data were acquired 14 d after siRNA injection. (B) Immunostaining of TA anterior cross sections. Bars, 50  $\mu$ m. (C) Myofiber size distribution. (D) Mean myofiber cross-sectional area. Data are means  $\pm$  SEM. \*,  $P < 0.05$  relative to siNC1.

on luciferase activity directed by either of those promoter sequences. However, addition of the 2.7-kb region containing the Chronos homology motifs led to a reduction in luciferase activity from both Bmp7 promoter constructs on d 1 of differentiation. Notably, addition of siChronos completely abrogated the repressive effects of the 2.7-kb Chronos homology region (Fig. 5 B). For further validation, the 2.7-kb region was inserted into a luciferase expression vector upstream of the heterologous SV40 promoter. When analyzed in proliferating myoblasts, the presence of the 2.7-kb region was sufficient to repress luciferase activity (Fig. 5 C). Luciferase activity was restored to  $\sim 50\%$  of control after 24 h of differentiation, and the addition of siChronos completely abrogated the inhibitory effects of the Chronos homology region. Together, these data indicate that the Chronos homology region upstream of Bmp7 functions as a Chronos-responsive transcriptional repressive element.

To extend those observations, we performed Pol II chromatin immunoprecipitation (ChIP) on nuclear extracts from proliferating and differentiating myoblasts. The RNA Pol

II occupancy of the Bmp7 TSS was observed to increase  $\sim 11.7$ -fold ( $4.9 \pm 1.7$  to  $57.7 \pm 6.6$  binding events per 1000 cells) in myoblasts on d 2 of differentiation in the presence of siChronos as compared with d-0 controls (Fig. 5 D). Those observations, consistent with the increase in Bmp7 expression after siChronos treatment in vitro (Fig. 3 C) and in vivo (Fig. 3 A), suggest that Chronos recruits an epigenetic modifier or transcriptional corepressor to the Bmp7 locus. To explore that possibility, a combination of RNA pull-down assays and candidate screens for RNA binding proteins was used (Fig. S3). Of the putative RNA binding proteins, Ezh2 was selected for subsequent analyses because it is known to be recruited to genomic loci by lncRNAs (Rinn et al., 2007; Gupta et al., 2010). Ezh2 ChIP analysis revealed a 68% decrease in Ezh2 occupancy of the -7885 site in differentiating myoblasts in the presence of siChronos as compared with the control (Fig. 5 E). No change in Ezh2 occupancy was observed at the -3389 site, thus indicating specificity. Although these luciferase reporter and ChIP data indicate that Chronos' repressive effects on Bmp7 transcription

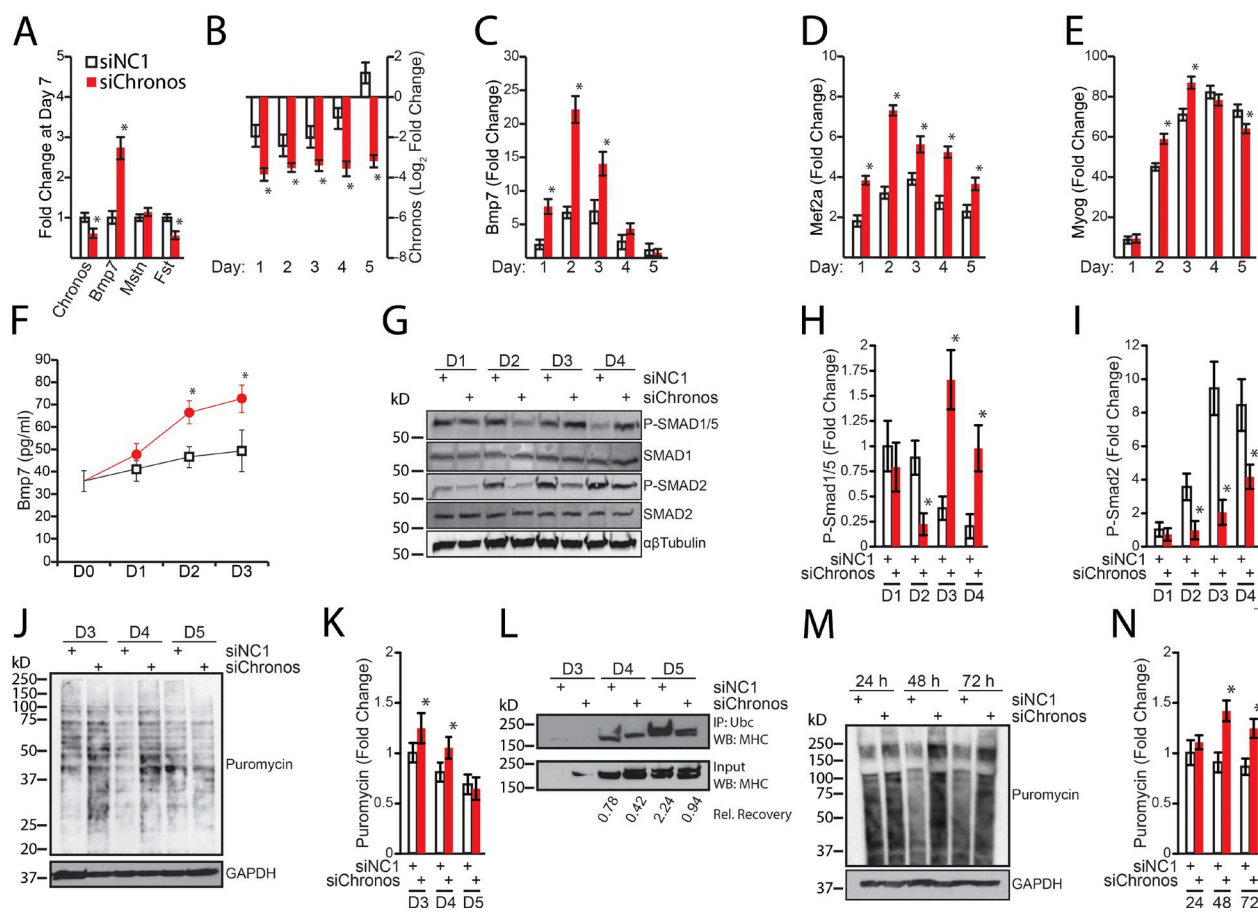


**Figure 3. Inhibition of Chronos activates hypertrophic signaling.** (A–N) Mean values are represented by white (siNC1) or red (siChronos) boxes or circles. Data are means  $\pm$  SD. \*,  $P < 0.05$ . (A) Analysis of gene expression from  $n = 6$  independent experiments. Samples were acquired 7 d after siRNA injection. (B–E) Data are presented normalized to gene expression at d 0 from  $n = 4$  independent experiments. (F) Quantification of secreted Bmp7 after 3 d differentiation. \*,  $P < 0.05$  from  $n = 8$  independent experiments. (G) Representative Western blots of the cells from F. (H and I) Quantification of the relative changes in Smad1/5 (H) and Smad2 (I) phosphorylation. (J) Representative Western blot of puromycin incorporation in differentiating myoblasts. (K) Quantification of J. (L) Immunoprecipitation of ubiquitinated myosin. (M) Representative Western blot of puromycin incorporation in mature myotubes. (N) Quantification of M. (J–K, M–N) Data are from  $n = 3$  independent experiments.

are dependent on the Chronos homology region, and mediated by *Ezh2*, further studies will be required to test whether the formation of a lncRNA:DNA heteroduplex is involved in the regulation of the *Bmp7* locus.

Experiments also tested whether Chronos overexpression was sufficient to inhibit myotube maturation and hypertrophy. Myoblasts transfected with Chronos 98–3259 or Chronos 1467–3259 displayed significantly impaired *Bmp7* induction as compared with empty vector controls (Fig. 5 F). Ectopic expression of Chronos 98–3259 or Chronos 1467–3259 similarly impaired and/or delayed the induction of *MyoG*, *Myh1*, and *Myh2* (Fig. 5, G–I). Finally, myoblasts transfected with Chronos 98–3259 or 1467–3259 exhibited impaired myogenesis as indicated by spindly MF20-positive cells with a paucity of nuclei as compared with empty vector control (Fig. 5 J). Importantly, myoblasts overexpressing Chronos phenocopy myoblasts treated with siBmp7 (Fig. 5 J).

Our findings identify Chronos as a muscle-enriched, Akt-inhibited, aging-related lncRNA that functions as an inhibitor of hypertrophic growth. Chronos, however, does not appear to function as a classical “atrogene” because its expression is uncoupled from the loss of muscle mass in models of acute atrophy. Physiologic maintenance of muscle mass is dependent on the proper balance of multiple signaling pathways, including

(a) the TGF- $\beta$  family, activins, and GDFs, including myostatin, which both inhibit Akt1 and lead to the activation of an atroge program via activation of Smad2/3 (Goodman and Hornberger, 2014; Cohen et al., 2015); and (b) BMPs and GDFs, which activate Akt1 to inhibit activation of an atroge program through activation of Smad1/5/8 (Sartori et al., 2013; Goodman and Hornberger, 2014). Our data indicate that Chronos functions to alter that balance, in part, through repression of Bmp7, and are consistent with prior studies documenting the hypertrophic effects of Bmp7 signaling in general (Sartori et al., 2013), and the Bmp7 ligand specifically (Winbanks et al., 2013). Although our data suggest a direct effect of Chronos on Bmp7 transcription, we cannot rule out the inhibitory effects of an unknown peptide encoded by Chronos. Future studies to identify potential Chronos-encoded micropeptides, additional Chronos-targeted loci, and its human homologue are of great interest.

## Materials and methods

### Mouse models

Inducible Akt1 transgenic mice have been previously described (Izumiya et al., 2008; Wu et al., 2017). In brief, constitutively active Akt1 transgenic mice (TRE-myrAkt1) were crossed with 1256[3Emut]

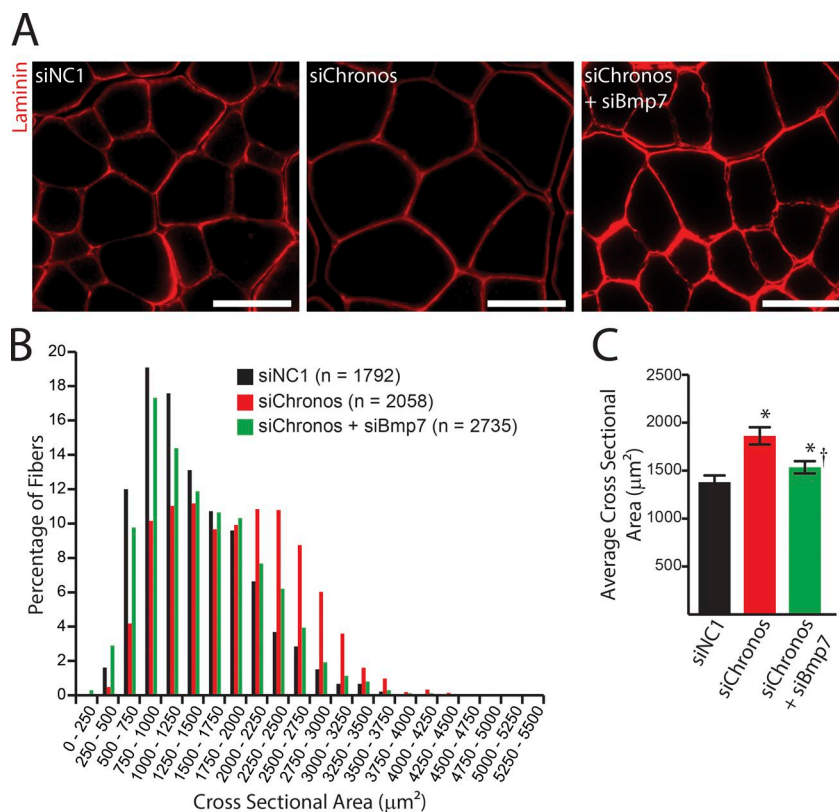


**Figure 4. Chronos inhibits hypertrophy through repression of Bmp7 in vivo.** (A) Immunostaining of TA cross sections. Bars, 50  $\mu\text{m}$ . (B) Myofiber size distribution. (C) Mean myofiber cross-sectional area. Data were acquired 14 d after siRNA injection. Data are means  $\pm$  SEM. \*,  $P < 0.05$  relative to siNC1; †,  $P < 0.05$  relative to siChronos.

MCK–reverse tetracycline transactivator (rtTA) transgenic mice. The 1256[3Emut]MCK promoter specifically expresses rtTA in type IIb glycolytic fibers. Transgene expression was activated by adding doxycycline (0.5 mg/ml) to the water.

Aged C57BL/6 mice were purchased from Charles River. Adult C57BL/6J mice were purchased from The Jackson Laboratory at 8–10 wk old and subjected to CTX injury, as previously described (Nepl et al., 2014) or injection of siRNA into the TA muscle, as previously described (Kinouchi et al., 2008). In brief, 40  $\mu\text{l}$  of 10  $\mu\text{M}$  CTX from *Naja mossambica mossambica* was injected into the TA muscle, whereas the contralateral TA muscle was injected with an equal volume of sterile saline. siRNAs were mixed with AteloCollagen (Koken Co.) at a final concentration of 10  $\mu\text{M}$ , according to the manufacturer's instructions. After anesthetizing, 30  $\mu\text{l}$  of the siRNA–AteloCollagen complex was injected into the TA muscle. The TA muscles were harvested and processed for analysis at 7 and 14 d after injection.

Hind limb unloading was performed on five 6-wk-old, female C57BL/6J mice for 7 d, as previously described (Wu et al., 2011). In brief, the adhesive surface of a folded strip of adhesive foam (AliMed) was loosely applied longitudinally along the proximal two-third of the tail of the anesthetized mice. Elastoplast tape was wrapped circumferentially around the adhesive foam, and a wire was inserted in between the fold of the adhesive foam and then drawn up to a pulley attached to a 360° swivel hook at the top of the cage. The length of the wire was adjusted such that the toes of the hind limbs touched the cage floor only during full hind limb extension. Gastrocnemius muscles were collected from unloaded mice and their littermates as weight-bearing controls for RNA isolation. Gastrocnemius muscle wet weight (in milligrams) was normalized to total body weight (in grams).

Type 1 diabetes was induced in 9-wk-old C57BL/6J mice, purchased from The Jackson Laboratory, with daily i.p. injections of streptozotocin (STZ). In brief, mice received a daily i.p. injection of STZ (50 mg/kg body weight) or an equal volume of saline buffer

for a consecutive 5 d. Fasting blood glucose levels were measured (Aviva Plus Accu-Chek blood glucose monitor) at 14-d after injection. STZ induced a significant increase in fasting blood glucose levels ( $387 \pm 30.4$  mg/ml,  $n = 6$ ,  $P < 0.001$ ) as compared with that of nondiabetic control mice ( $111.7 \pm 5.7$  mg/ml,  $n = 6$ ). Gastrocnemius muscles wet weight (in milligrams) was normalized to tibia length (in centimeters). All experiments were performed in adherence with National Institutes of Health guidelines on the use of laboratory animals and were approved by the Institutional Animal Care and Use Committee at Boston University.

#### RNAseq

High-throughput RNA sequencing was performed on poly A+ RNA-derived cDNA of gastrocnemius muscles from double transgenic mice (1256[3Emut]MCK–rtTA  $\times$  TRE–myrAkt1) and their MCK–rtTA littermates treated with 2 wk of doxycycline water (Izumiya et al., 2008). RNAseq methodology, statistical analysis, and the data set have been previously described (Wu et al., 2017). In brief, we used RSEM to identify transcripts in each sample and edgeR software (Bioconductor) for differential gene expression analysis. Transcripts expression altered  $\geq 1.5$ -fold or  $\leq -1.5$ -fold or less,  $P < 0.05$ , and a false-discovery rate of  $< 0.05$  were considered statistically different between the two groups. The UCSC Genome Database (University of California, Santa Cruz) was used as a reference to identify differentially expressed transcripts. Only those transcripts annotated as noncoding RNA were screened further.

#### Cell culture, siRNA

C2C12 cells were purchased from ATCC, and all experiments were performed with cells at a passage  $< 10$ . Cells were maintained in growth medium consisting of DMEM supplemented with 10% FBS (vol/vol). To induce differentiation, cells were grown to  $\sim 70\%$  confluency; at which point, the medium was changed to differentiation medium consisting of

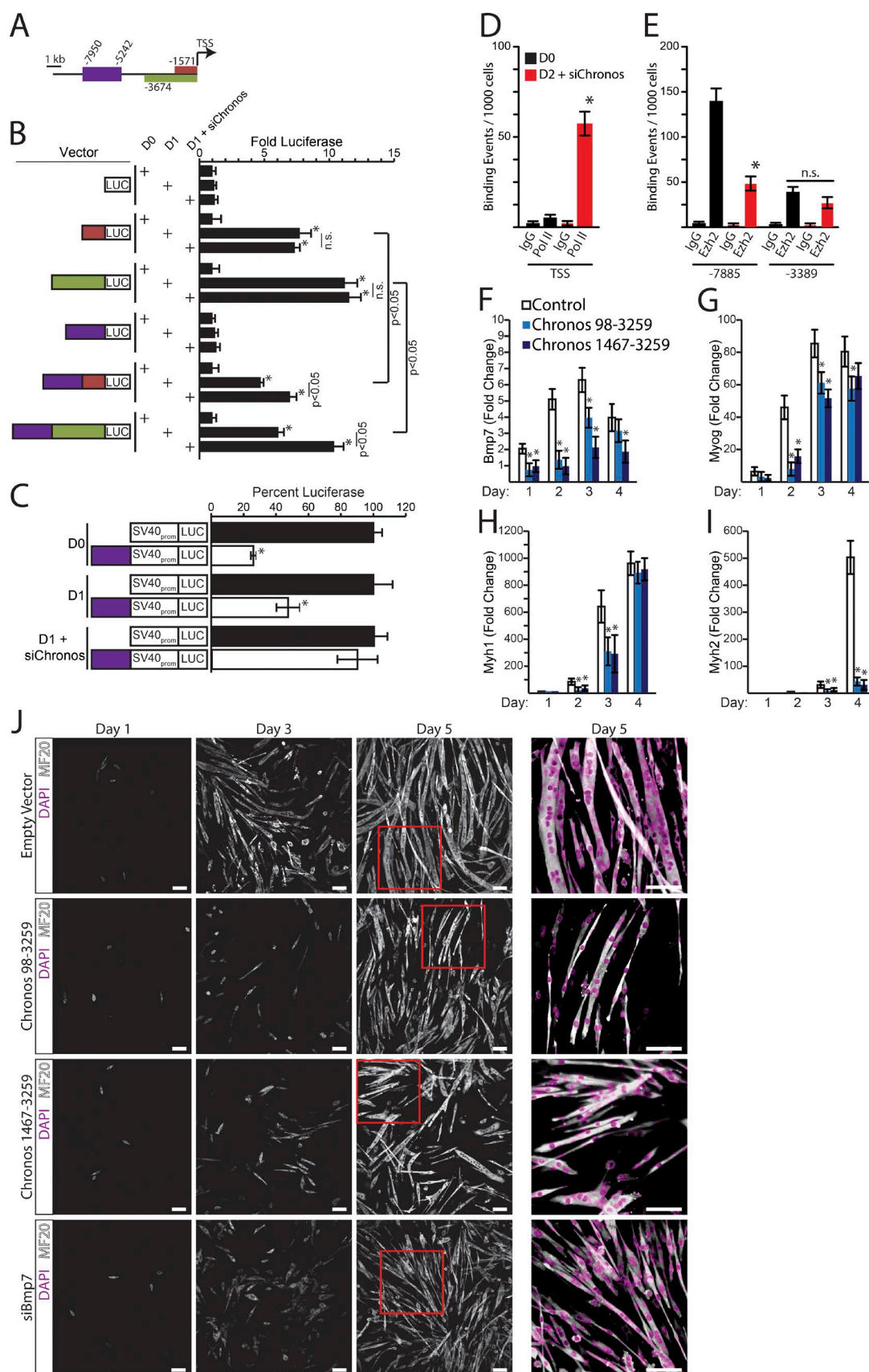


**Figure 5. Chronos regulates Bmp7 transcription via an upstream repressor.** (A–C) Chronos response region (purple). Bmp7 promoters of -1571 to +3 (orange) and -3674 to +3 (green). (A) Schematic of Bmp7 locus. (B and C) Luciferase reporter assay in proliferating myoblasts (d 0) and after 24 h of differentiation (d 1) ± siChronos. Data are means ± SD from  $n = 8$  independent experiments. \*,  $P < 0.05$  relative to d 0. (B) Luciferase activities driven

### Quantitative real-time PCR

qF1 5'-GCTGCGCCATGAAAACATCC-3', Acvr1b qR1 5'-GTC  
TGCAATGGCACACATGC-3', Acvr2b qF1 5'-CATGAGGTGAGA  
CAGTGCCAG-3', Acvr2b qR1 5'-AGATTTCCTTCCTACTCT  
GCC-3', Igfr1 qF1 5'-GCGAGCCTGGCATTCTTACTG-3', Igfr1 qR1  
5'-TTGGAGCAGTAGTTGTGCCG-3', Slc2a4 qF1 5'-ATCTTGATG  
ACCGTGGCTCTG-3', Slc2a4 qR1 5'-TGAGATCTGGTCAAACG  
CCG-3', Foxo1 qF1 5'-TCAAGGATAAGGGCGACAGC-3', Foxo1  
qR1 5'-CTCGAGGCCACTTAGAAAAAC-3', Fbxo32 qF1 5'-GTG  
GCATCGCCCAAAAAGAAC-3', Fbxo32 qR1 5'-TGTAAGCACACA  
GGCAGGTC-3', Hdac4 qF1 5'-TGTCTGCTCTGTGGGAAAC-3',  
Hdac4 qR1 5'-TGCGCCTCAATCAGAGAGTG-3', Cryab qF1  
5'-TGACCTCTTCTCAACAGCCAC-3', Cryab qR1 5'-TCCCC  
AGAACCTTGACTTTG-3', Psmc3 qF1 5'-ATTGAGTTTCCAATG  
CCCAACG-3', Psmc3 qR1 5'-GGACAGACTAGAGGTGTCCCC.  
Pacsin3 qF1 5'-TTTCCGTAAAGCTCAGAAGCCC-3', Pacsin3 qR1  
5'-CATGTAGCGTGGGGTGATAGC-3', Atg13 qF1 5'-GATTTGCAC  
CCGCTCATCATC-3', Atg13 qR1 5'-GCCTCTTTTGCTTCATGG  
GTG-3', Atp6ap2 qF1 5'-TCTCCGAAGTCAAGTGCTAC-3', Atp-  
6ap2 qR1 5'-CACTGCGTTCCTCCACCATAGAG-3', Ambral qF1  
5'-TGCTTCTGGTTGCCTAGATGG-3', Ambral qR1 5'-TGAAA  
GCCAAGGAGGCTATG-3', Med14 qF1 5'-TGGAATGTCACCAGC  
TAACCC-3', Med14 qR1 5'-AGGAGCGCTGAGGTAGTTTTC-3',  
Mef2a qF1 5'-TTTTTAAGACAATTTCAACGGCAGC-3', Mef2a  
qR1 5'-ATCCGAGTTTCGTCTGCTTTC-3', Myog qF1 5'-TAC  
AGGCCTTGCTCAGCTCC-3', Myog qR1 5'-TGTGGGAGTTGC  
ATTCAGTG-3', Myh1 qF1 5'-ACGGTCAAGTTGCATCCC-3',  
Myh1 qR1 5'-TTCTGAGCCTCGATTCGCTC-3', Myh2 qF1  
5'-ATATAAAAAGAGTCCCCGAACGAGGC-3', Mhy2 qR1 5'-TCT  
GGTCTTCTTTCAAGGTCA-3'.

### Luciferase reporter assay

Genomic regions upstream of mouse *Bmp7* TSS were inserted upstream of Luc in either the pGL3-Basic Vector (Promega) or pISO (Addgene) containing the SV40 promoter/enhancer flanking Luc. Mouse *Bmp7* promoter regions were amplified using forward (-3674) 5'-GCAGTTCAGACACAATGAC-3', forward (-1571) 5'-CCCTCAGACAGTCACATCACC-3', and reverse (+3) 5'-CAAGGCTAGCACAGCAACTC-3'. Chronos recognition region was amplified using forward (-7950) 5'-TGA GAAAATCCCCATGTCCCC-3' and reverse (-5242) 5'-ACTCTCCATGAAGGGCCAAAC-3' and inserted upstream of Luc in both pGL3-Basic and pISO. 2C12 were transfected with equal amounts of plasmid DNA using Lipofectamine 2000 (Thermo Fisher Scientific). Renilla luciferase (pRL-TK) was used as a normalization control. The dual-luciferase reporter assay system (Promega) was used for quantification.

## ChIP

ChIP was performed according to the ChIP-IT kit protocol (Active Motif). Control IgG, RNA Pol II, and Ezh2 antibodies were from Active Motif. Control ChIP primers toward glyceraldehyde 3-phosphate dehydrogenase (GAPDH) were from Active Motif. Primer sequences included forward (-7885) 5'-GCAACAGTTAGCATCATGGGC-3', reverse (-7885) 5'-TGGGGTTGTAGGCTTTCCTG-3', forward (-3389) 5'-CAGGGCATGGCTGTTTGATG-3', reverse (-3389) 5'-CAGGTG CATGGGGTACAGAG-3', forward (TSS) 5'-CGGAAAGGGGGTTTGT TGCTGG-3', reverse (TSS) 5'-GGGACGCCCTGTCTTTTAC-3'.

Downloaded from [http://rupress.org/jcb/article-pdf/216/11/3497/1604370/jcb\\_201612100.pdf](http://rupress.org/jcb/article-pdf/216/11/3497/1604370/jcb_201612100.pdf) by guest on 05 December 2025

### Plasmids and pull-down assays

C2C12 cells were transfected with Myc-tagged Ddx3x (NM\_010028.3), Ddx5 (NM\_007840.3), DGCR8 (NM\_001190326.1), Ezh2 (NM\_007971.2), Fus (NM\_139149.2), Fxr1 (NM\_008053.2), Stau1 (NM\_017453.3), Chronos 98-3259, Chronos 1467-3259, or pcDNA3.1<sup>+</sup> using Lipofectamine 2000 (Thermo Fisher Scientific). Chronos 98-3259 and Chronos 1467-3259 were cloned into the pcDNA3.1<sup>+</sup> vector. Cells were lysed in 10 mM Hepes, pH 7.9; 100 mM KCl; 2 mM MgCl<sub>2</sub>; 0.2 mM DTT; 200 U/ml RNase inhibitor; 1 mM ATP; 0.2 mM GTP; and 0.5% Triton X-100 and cleared by centrifugation at 10,000 g for 10 min at 4°C. Cleared lysates were diluted 1:3 with lysis buffer and incubated with EZview RED anti-c-Myc affinity gel (Sigma-Aldrich) at 4°C for 6 h with gentle rocking. Beads were subsequently washed five times with lysis buffer. C0mplete EDTA-free protease inhibitor (Roche) was present in all solutions from initial lysis to final wash. For protein analysis, beads were resuspended in 50 µl of 2× Laemmli buffer and stored at −20°C until size separation by SDS-PAGE and Western blot analysis. For RNA analysis, beads were resuspended in 1 ml of TRIzol (Thermo Fisher Scientific), and RNA was purified according to manufacturer's protocol. One-half of the RNA was reverse transcribed using random primers, and the other half was reserved as a negative control.

### Nuclear extracts

Nuclear extracts were prepared according to previously described methods (Nabbi and Riabowol, 2015). In brief, the pellet of ~6 × 10<sup>6</sup> nonconfluent C2C12 cells were resuspended in ice-cold 0.1% NP-40 in PBS and centrifuged for 30 s at 10,000 g at 4°C. The pelleted nuclear fraction was resuspended in 1 ml RNA immunoprecipitation (RIP) buffer (150 mM KCl, 25 mM Tris pH 7.4, 0.5 mM DTT, 0.5% NP-40, and 1 mM PMSF) supplemented with C0mplete EDTA-free protease inhibitor and incubated on ice for 30 min with periodic vortexing. Nuclear debris was removed by centrifugation at 13,000 g for 10 min at 4°C.

### RNA pull-down assay

RNA pull-down was performed according to previously described methods (Wang et al., 2015). In brief, biotinylated RNAs were prepared using SP6 and T7 RNA polymerases (Roche) with biotin-16-uridine-5'-triphosphate (Bio-16-UTP; Invitrogen). RNAs were incubated at 90°C for 2 min and then placed on ice for 2 min. An equal volume of 2× RNA structure buffer (20 mM Tris HCL, pH 7.4; 0.2 M KCl; 20 mM MgCl<sub>2</sub>; 2 mM DTT; 0.8 U/µl RNase inhibitor) was added and incubated at RT for 20 min. Approximately 750–1000 µg of nuclear extract was mixed with ~2.5 µg of RNA and incubated for 1 h at RT with rocking. 25 µl of washed streptavidin agarose beads (Invitrogen) was added and incubated for 1 h at RT with rocking. Beads were pelleted and washed five times with RIP buffer (150 mM KCl; 25 mM Tris, pH 7.4; 0.5 mM DTT; 0.5% NP-40; 1 mM PMSF) supplemented with protease inhibitor. Beads were resuspended in 50 µl of 2× Laemmli buffer and stored at −20°C until size separation by SDS-PAGE and Coomassie staining.

### Motif analysis

De novo motif analysis was performed in silico using MEME software at (<http://meme-suite.org>; The MEME Suite).

### ELISA

Secreted mouse Bmp7 was quantified by sandwich ELISA according to manufacturer's protocol (LifeSpan BioSciences).

### Western blot analysis

Cells were homogenized in 40 mM Tris, pH 7.4; 150 mM NaCl; 1% Triton X-100; and C0mplete EDTA-free protease inhibitor cocktail

(Roche). Protein content was determined by the DC protein assay (Bio-Rad Laboratories) with known concentrations of BSA as standards. Protein concentrations were equalized by addition of an appropriate volume of lysis buffer. Primary antibody was visualized with HRP-conjugated goat anti-mouse and anti-rabbit secondary antibodies. Quantification was performed with ImageJ software (National Institutes of Health).

### Protein synthesis analysis

Puromycin (Millipore Sigma) was added to cell culture medium to a final concentration of 1 µM and incubated for 30 min as previously described (Goodman et al., 2011). At that dose, puromycin incorporation into neosynthesized proteins reflects the rate of mRNA translation in vitro (Schmidt et al., 2009). Puromycin incorporation was detected by Western blot analysis.

### Antibodies

Rabbit anti-phospho Smad1/5, rabbit anti-phospho Smad2, rabbit anti-Smad1/5, rabbit anti-Smad2, and rabbit anti-α/β tubulin antibodies were purchased from Cell Signaling Technology. Mouse anti-laminin antibodies were purchased from Sigma-Aldrich. Mouse anti-myosin (MF20) antibody was purchased from the Developmental Studies Hybridoma Bank at the University of Iowa. Rabbit anti-ubiquitin antibody was purchased from Abcam. Mouse Anti-GAPDH and mouse anti-puromycin antibodies were purchased from Millipore Sigma.

### Immunohistochemistry and histologic analysis

Hind limb muscles were excised, fixed in 4% PFA, cryoprotected with 30% sucrose, and embedded in Tissue-Tek optimum cutting temperature formulation. Sections were cut transversely and subjected to immunostaining and nuclei counterstain with DAPI. C2C12 myoblasts were fixed in 4% PFA and subjected to immunostaining and nuclei counterstain with DAPI. Fixed tissues and cells were permeabilized with 0.05% Triton X-100 for 20 min and blocked with 5% normal donkey serum. Primary antibodies were visualized with cyanine Cy3 or Alexa-Fluor 594 conjugated donkey anti-mouse antibodies from Jackson ImmunoResearch Laboratories. Coverslips were mounted with Aqua-Poly/Mount (Polysciences) or Vectashield (Vector Laboratories). All images were acquired at RT with a BZ-9000 fluorescence microscope (KEYENCE) using either a 10× PlanApo (NA 0.45) or a 20× PlanApo (NA 0.75) objective with the BZ-II Analyzer software (KEYENCE). Approximately 10–15 images were acquired from each transverse section. Myofiber cross-sectional areas were calculated using BZ-II Analyzer software or CellProfiler (Jones et al., 2008).

### Image processing

Acquired images were minimally processed in Photoshop (Adobe). Contrast was enhanced with auto-contrast function on the whole-image file. Nuclei were false colored and overlaid onto the MF20 image with either the color or soft-light layer function.

### Statistical methods

Data are presented as means ± SD unless indicated otherwise. Two-tailed, unpaired Student's *t* tests or two-way ANOVA were performed on experimental data from at least three individual experiments.

### Online supplemental material

Fig. S1 shows changes in the in vivo gene expression on d 7 after the injection of siChronos. Fig. S2 shows a schematic diagram of the Bmp7 locus and in silico analyses depicting the putative Chronos homology motif. Fig. S3 displays tandem mass spectrometry identification of RNA binding proteins precipitating with biotinylated Chronos and in vitro validation of the putative targets.

## Acknowledgments

This work was funded by National Institutes of Health grants HL120160, HL132564, HL129120, and AG052160 to K. Walsh.

The authors declare no competing financial interests.

Author contributions: R.L. Neppl and C.L. Wu performed the research. R.L. Neppl, C.L. Wu, and K. Walsh designed experiments. R.L. Neppl and K. Walsh wrote the manuscript.

Submitted: 14 December 2016

Revised: 28 June 2017

Accepted: 3 August 2017

## References

- Akasaki, Y., N. Ouchi, Y. Izumiya, B.L. Bernardo, N.K. LeBrasseur, and K. Walsh. 2014. Glycolytic fast-twitch muscle fiber restoration counters adverse age-related changes in body composition and metabolism. *Aging Cell*. 13:80–91. <http://dx.doi.org/10.1111/ace.12153>
- Bodine, S.C., T.N. Stitt, M. Gonzalez, W.O. Kline, G.L. Stover, R. Bauerlein, E. Zlotchenko, A. Scrimgeour, J.C. Lawrence, D.J. Glass, and G.D. Yancopoulos. 2001. Akt/mTOR pathway is a crucial regulator of skeletal muscle hypertrophy and can prevent muscle atrophy in vivo. *Nat. Cell Biol.* 3:1014–1019. <http://dx.doi.org/10.1038/ncb1101-1014>
- Ciciliot, S., A.C. Rossi, K.A. Dyar, B. Blaauw, and S. Schiaffino. 2013. Muscle type and fiber type specificity in muscle wasting. *Int. J. Biochem. Cell Biol.* 45:2191–2199. <http://dx.doi.org/10.1016/j.biocel.2013.05.016>
- Clever, J.L., Y. Sakai, R.A. Wang, and D.B. Schneider. 2010. Inefficient skeletal muscle repair in inhibitor of differentiation knockout mice suggests a crucial role for BMP signaling during adult muscle regeneration. *Am. J. Physiol. Cell Physiol.* 298:C1087–C1099. <http://dx.doi.org/10.1152/ajpcell.00388.2009>
- Cohen, S., J.A. Nathan, and A.L. Goldberg. 2015. Muscle wasting in disease: Molecular mechanisms and promising therapies. *Nat. Rev. Drug Discov.* 14:58–74. <http://dx.doi.org/10.1038/nrd4467>
- Gong, C., Z. Li, K. Ramanujan, I. Clay, Y. Zhang, S. Lemire-Brachat, and D.J. Glass. 2015. A long non-coding RNA, lncMyoD, regulates skeletal muscle differentiation by blocking IMP2-mediated mRNA translation. *Dev. Cell*. 34:181–191. <http://dx.doi.org/10.1016/j.devcel.2015.05.009>
- Goodman, C.A., and T.A. Hornberger. 2014. New roles for Smad signaling and phosphatidic acid in the regulation of skeletal muscle mass. *F1000Prime Rep.* 6:20. <http://dx.doi.org/10.12703/P6-20>
- Goodman, C.A., D.M. Mabrey, J.W. Frey, M.H. Miu, E.K. Schmidt, P. Pierre, and T.A. Hornberger. 2011. Novel insights into the regulation of skeletal muscle protein synthesis as revealed by a new nonradioactive in vivo technique. *FASEB J.* 25:1028–1039. <http://dx.doi.org/10.1096/fj.10-168799>
- Gupta, R.A., N. Shah, K.C. Wang, J. Kim, H.M. Horlings, D.J. Wong, M.C. Tsai, T. Hung, P. Argani, J.L. Rinn, et al. 2010. Long non-coding RNA HOT AIR reprograms chromatin state to promote cancer metastasis. *Nature*. 464:1071–1076. <http://dx.doi.org/10.1038/nature08975>
- Guttman, M., J. Donaghey, B.W. Carey, M. Garber, J.K. Grenier, G. Munson, G. Young, A.B. Lucas, R. Ach, L. Bruhn, et al. 2011. lincRNAs act in the circuitry controlling pluripotency and differentiation. *Nature*. 477:295–300. <http://dx.doi.org/10.1038/nature10398>
- Guttman, M., P. Russell, N.T. Ingolia, J.S. Weissman, and E.S. Lander. 2013. Ribosome profiling provides evidence that large noncoding RNAs do not encode proteins. *Cell*. 154:240–251. <http://dx.doi.org/10.1016/j.cell.2013.06.009>
- Hu, W., J.R. Alvarez-Dominguez, and H.F. Lodish. 2012. Regulation of mammalian cell differentiation by long non-coding RNAs. *EMBO Rep.* 13:971–983. <http://dx.doi.org/10.1038/embor.2012.145>
- Iyer, M.K., Y.S. Niknafs, R. Malik, U. Singhal, A. Sahu, Y. Hosono, T.R. Barrette, J.R. Prensner, J.R. Evans, S. Zhao, et al. 2015. The landscape of long noncoding RNAs in the human transcriptome. *Nat. Genet.* 47:199–208. <http://dx.doi.org/10.1038/ng.3192>
- Izumiya, Y., T. Hopkins, C. Morris, K. Sato, L. Zeng, J. Viereck, J.A. Hamilton, N. Ouchi, N.K. LeBrasseur, and K. Walsh. 2008. Fast/glycolytic muscle fiber growth reduces fat mass and improves metabolic parameters in obese mice. *Cell Metab.* 7:159–172. <http://dx.doi.org/10.1016/j.cmet.2007.11.003>
- Jones, T.R., I.H. Kang, D.B. Wheeler, R.A. Lindquist, A. Papallo, D.M. Sabatini, P. Golland, and A.E. Carpenter. 2008. CellProfiler Analyst: Data exploration and analysis software for complex image-based screens. *BMC Bioinformatics*. 9:482. <http://dx.doi.org/10.1186/1471-2105-9-482>
- Kawakami, E., N. Kawai, N. Kinouchi, H. Mori, Y. Ohsawa, N. Ishimaru, Y. Sunada, S. Noji, and E. Tanaka. 2013. Local applications of myostatin-siRNA with atelocollagen increase skeletal muscle mass and recovery of muscle function. *PLoS One*. 8:e64719. <http://dx.doi.org/10.1371/journal.pone.0064719>
- Khalil, A.M., M. Guttman, M. Huarte, M. Garber, A. Raj, D. Rivea Morales, K. Thomas, A. Presser, B.E. Bernstein, A. van Oudenaarden, et al. 2009. Many human large intergenic noncoding RNAs associate with chromatin-modifying complexes and affect gene expression. *Proc. Natl. Acad. Sci. USA*. 106:11667–11672. <http://dx.doi.org/10.1073/pnas.0904715106>
- Kinouchi, N., Y. Ohsawa, N. Ishimaru, H. Ohuchi, Y. Sunada, Y. Hayashi, Y. Tanimoto, K. Moriyama, and S. Noji. 2008. Atelocollagen-mediated local and systemic applications of myostatin-targeting siRNA increase skeletal muscle mass. *Gene Ther.* 15:1126–1130. <http://dx.doi.org/10.1038/gt.2008.24>
- Lai, K.M., M. Gonzalez, W.T. Poueymirou, W.O. Kline, E. Na, E. Zlotchenko, T.N. Stitt, A.N. Economides, G.D. Yancopoulos, and D.J. Glass. 2004. Conditional activation of akt in adult skeletal muscle induces rapid hypertrophy. *Mol. Cell Biol.* 24:9295–9304. <http://dx.doi.org/10.1128/MCB.24.21.9295-9304.2004>
- LeBrasseur, N.K., K. Walsh, and Z. Arany. 2011. Metabolic benefits of resistance training and fast glycolytic skeletal muscle. *Am. J. Physiol. Endocrinol. Metab.* 300:E3–E10. <http://dx.doi.org/10.1152/ajpendo.00512.2010>
- Lee, J.T. 2012. Epigenetic regulation by long noncoding RNAs. *Science*. 338:1435–1439. <http://dx.doi.org/10.1126/science.1231776>
- Miyazono, K., K. Kusanagi, and H. Inoue. 2001. Divergence and convergence of TGF- $\beta$ /BMP signaling. *J. Cell. Physiol.* 187:265–276. <http://dx.doi.org/10.1002/jcp.1080>
- Mousavi, K., H. Zare, S. Dell'orso, L. Grontved, G. Gutierrez-Cruz, A. Derfoul, G.L. Hager, and V. Sartorelli. 2013. eRNAs promote transcription by establishing chromatin accessibility at defined genomic loci. *Mol. Cell*. 51:606–617. <http://dx.doi.org/10.1016/j.molcel.2013.07.022>
- Mueller, A.C., M.A. Cichewicz, B.K. Dey, R. Layer, B.J. Reon, J.R. Gagan, and A. Dutta. 2015. MUNC, a long noncoding RNA that facilitates the function of MyoD in skeletal myogenesis. *Mol. Cell Biol.* 35:498–513. <http://dx.doi.org/10.1128/MCB.01079-14>
- Nabbi, A., and K. Riabowol. 2015. Rapid isolation of nuclei from cells in vitro. *Cold Spring Harb. Protoc.* 2015:769–772. <http://dx.doi.org/10.1101/pdb.prot083733>
- Neppl, R.L., M. Kataoka, and D.Z. Wang. 2014. Crystallin- $\alpha$ B regulates skeletal muscle homeostasis via modulation of argonaute2 activity. *J. Biol. Chem.* 289:17240–17248. <http://dx.doi.org/10.1074/jbc.M114.549584>
- O'Leary, V.B., S. Hain, D. Mugg, J. Smida, O. Azimzadeh, S. Tapio, S.V. Ovsepian, and M.J. Atkinson. 2017. Long non-coding RNA *PARTIC LE* bridges histone and DNA methylation. *Sci. Rep.* 7:1790. <http://dx.doi.org/10.1038/s41598-017-01875-1>
- Pisignano, G., S. Napoli, M. Magistri, S.N. Mapelli, C. Pastori, S. Di Marco, G. Civenni, D. Albino, C. Enriquez, S. Allegrini, et al. 2017. A promoter-proximal transcript targeted by genetic polymorphism controls E-cadherin silencing in human cancers. *Nat. Commun.* 8:15622. <http://dx.doi.org/10.1038/ncomms15622>
- Rinn, J.L., M. Kertes, J.K. Wang, S.L. Squazzo, X. Xu, S.A. Brugmann, L.H. Goodnough, J.A. Helms, P.J. Farnham, E. Segal, and H.Y. Chang. 2007. Functional demarcation of active and silent chromatin domains in human HOX loci by noncoding RNAs. *Cell*. 129:1311–1323. <http://dx.doi.org/10.1016/j.cell.2007.05.022>
- Rommel, C., S.C. Bodine, B.A. Clarke, R. Rossman, L. Nunez, T.N. Stitt, G.D. Yancopoulos, and D.J. Glass. 2001. Mediation of IGF-1-induced skeletal myotube hypertrophy by PI3K/Akt/mTOR and PI3K/Akt/GSK3 pathways. *Nat. Cell Biol.* 3:1009–1013. <http://dx.doi.org/10.1038/ncb1101-1009>
- Sartori, R., G. Milan, M. Patron, C. Mammucari, B. Blaauw, R. Abraham, and M. Sandri. 2009. Smad2 and 3 transcription factors control muscle mass in adulthood. *Am. J. Physiol. Cell Physiol.* 296:C1248–C1257. <http://dx.doi.org/10.1152/ajpcell.00104.2009>
- Sartori, R., E. Schirwis, B. Blaauw, S. Bortolanza, J. Zhao, E. Enzo, A. Stantzou, E. Mouisel, L. Toniolo, A. Ferry, et al. 2013. BMP signaling controls muscle mass. *Nat. Genet.* 45:1309–1318. <http://dx.doi.org/10.1038/ng.2772>
- Schmidt, E.K., G. Clavarino, M. Ceppi, and P. Pierre. 2009. SUNSET, a nonradioactive method to monitor protein synthesis. *Nat. Methods*. 6:275–277. <http://dx.doi.org/10.1038/nmeth.1314>
- Takahashi, A., Y. Kureishi, J. Yang, Z. Luo, K. Guo, D. Mukhopadhyay, Y. Ivashchenko, D. Branellec, and K. Walsh. 2002. Myogenic Akt signaling regulates blood vessel recruitment during myofiber growth.

- Mol. Cell. Biol.* 22:4803–4814. <http://dx.doi.org/10.1128/MCB.22.13.4803-4814.2002>
- Wang, L., Y. Zhao, X. Bao, X. Zhu, Y.K. Kwok, K. Sun, X. Chen, Y. Huang, R. Jauch, M.A. Esteban, et al. 2015. LncRNA Dum interacts with Dnmts to regulate Dppa2 expression during myogenic differentiation and muscle regeneration. *Cell Res.* 25:335–350. <http://dx.doi.org/10.1038/cr.2015.21>
- Winbanks, C.E., J.L. Chen, H. Qian, Y. Liu, B.C. Bernardo, C. Beyer, K.I. Watt, R.E. Thomson, T. Connor, B.J. Turner, et al. 2013. The bone morphogenetic protein axis is a positive regulator of skeletal muscle mass. *J. Cell Biol.* 203:345–357. <http://dx.doi.org/10.1083/jcb.201211134>
- Wu, C.L., S.C. Kandarian, and R.W. Jackman. 2011. Identification of genes that elicit disuse muscle atrophy via the transcription factors p50 and Bcl-3. *PLoS One.* 6:e16171. <http://dx.doi.org/10.1371/journal.pone.0016171>
- Wu, C.L., Y. Satomi, and K. Walsh. 2017. RNA-seq and metabolomic analyses of Akt1-mediated muscle growth reveals regulation of regenerative pathways and changes in the muscle secretome. *BMC Genomics.* 18:181. <http://dx.doi.org/10.1186/s12864-017-3548-2>
- Zeng, L., Y. Akasaki, K. Sato, N. Ouchi, Y. Izumiya, and K. Walsh. 2010. Insulin-like 6 is induced by muscle injury and functions as a regenerative factor. *J. Biol. Chem.* 285:36060–36069. <http://dx.doi.org/10.1074/jbc.M110.160879>